Polar Cap Electron Densities From DE 1 Plasma Wave Observations

Ann M. Persoon, Donald A. Gurnett, and Stanley D. Shawhan

Department of Physics and Astronomy, The University of Iowa

Electric field spectrum measurements from the plasma wave instrument on the Dynamics Explorer 1 spacecraft are used to study the local electron density at high altitudes in the northern polar cap region. The electron density is determined from the upper cutoff of whistler mode radiation at the electron plasma frequency. Median density values over the polar cap at L greater than 10 are found to vary from 35.2 ± 8.5 cm^{-3} at 2.1 R_E to 0.99 ± 0.51 cm^{-3} at 4.66 R_E. The steady state radial outflow model is examined for consistency with the observed density profile. A power law fit to the radial variation of the electron density yields an exponent of -3.85 ± 0.32, which for the radial outflow model implies a flow velocity increasing nearly linearly with increasing radial distance. Comparison of the observed electron densities with theoretical polar wind densities yields consistent results up to 2.8 R_E. A comparison of the observed electron densities with low-altitude density profiles from the Alouette II and ISIS 1 spacecraft illustrate transitions in the slope of the profile at 1.16 R_E and between 1.55 and 2.0 R_E. The changes in the density profile suggest that changes occur in the basic radial transport processes at these altitudes.

1. Introduction

In this report the electron density profile as a function of radial distance is determined by using electric field spectrum measurements from the plasma wave instrument on the Dynamics Explorer 1 spacecraft. The region of interest in this study is the earth's northern polar cap region where geomagnetic field lines open into the magnetotail and a steady outward plasma flow occurs. The polar cap region is defined to be the region of the magnetosphere poleward of the auroral field lines. For purpose of this study, the northern polar cap region was taken to be that region of the magnetosphere with L shell values greater than 10, corresponding to invariant latitudes greater than $71.6°$ ($\Lambda = \cos^{-1}(1/L)^{1/2}$).

Electron density measurements in the lower polar ionosphere have been made by a variety of direct and indirect techniques [*Thrane*, 1972]. Density data for high geomagnetic latitudes have been obtained by ground-based methods such as partial reflection, incoherent scatter radar, wave interaction, and ionosonde measurements [*Knight*, 1972]. Rocket measurements, including in situ probe measurements and measurements based on wave propagation effects, began in the late 1940's and were used to construct vertical electron density profiles to altitudes above the F_2 peak [*Knight*, 1972]. However, few rocket launching sites were located north of $60°$ geographic latitude in Alaska, Canada, and Scandinavia and the major interest in electron density profiles was in the low and middle latitudes [*Maeda*, 1969, 1971].

Satellites in eccentric and circular polar orbits, with orbit inclination angles exceeding $75°$ and apogees varying from a few hundred kilometers to several thousand kilometers, were able to obtain electron density measurements with more extensive spatial coverage of the northern polar cap region. Satellite density measurements were obtained by a variety of techniques which included in situ probe measurements and measurements based on wave propagation effects. The latter method was employed by the topside sounder satellites. Explorer 20 and four topside sounder satellites of the Allouette-ISIS series were launched in the decade following 1961 [*Calvert and Van Zandt*, 1966; *Florida* 1969; *Jackson and Warren*,

1969]. Electron density measurements obtained from the topside sounder data were used to construct electron density profiles up to 3500 km.

In situ probe measurements at high polar latitudes were obtained by a succession of American and European satellites launched in the late 1960's and early 1970's. Explorer 31 was launched in 1965 along with the topside sounder satellite Alouette II in order to provide simultaneous measurements of ionospheric plasma density by direct measurement probes and the topside sounder technique [*Donley et al.*, 1969]. The ESRO spacecraft, also in eccentric polar orbits with apogees exceeding 1100 km, provided direct electron density measurements for high-latitude density profiles [*Raitt*, 1971]. Satellites in circular polar orbits, including Explorer 22 [*Brace et al.*, 1970; *Miller and Brace*, 1969; *Reddy et al.*, 1969] and the Ariel spacecraft [*Sayers et al.*, 1969; *Tulunay*, 1972] were able to obtain information on latitudinal and diurnal variations in the electron density profile, as well as variations in the electron density with disturbances in the earth's magnetic field. Collectively, these polar orbiting satellites provided in situ electron density measurements up to 3000 km at high polar latitudes.

In 1974 and 1976, two spacecraft, Hawkeye I and S3-3, were launched into higher altitude orbits over the polar cap. The S3-3 satellite, with an apogee of 8000 km, carried instrumentation to measure electron densities both by the in situ probe technique and indirectly by the measurement of the upper hybrid resonance frequency [*Mozer et al.*, 1979]. However, although the data are available, no electron density measurements in the polar cap region have yet been published. The Hawkeye I spacecraft, with a polar apogee of 20.5 R_E, obtained electric and magnetic field measurments at large radial distances from 8 R_E to 20 R_E in the polar cap region [*Gurnett and Frank*, 1978]. Although density measurements at these altitudes could be derived from the Hawkeye electric field measurements [*Calvert*, 1981], to date no such results have been published.

The Dynamics Explorer 1 spacecraft, launched on August 3, 1981, is in an eccentric polar orbit with perigee and apogee geocentric radial distances of 1.09 R_E and 4.66 R_E, respectively. Because of the eccentricity and the latitudinal precession of the orbit, this spacecraft provides electric and magnetic field measurements over a region of the polar magnetosphere not previously studied. Figure 1 illustrates the orientation of

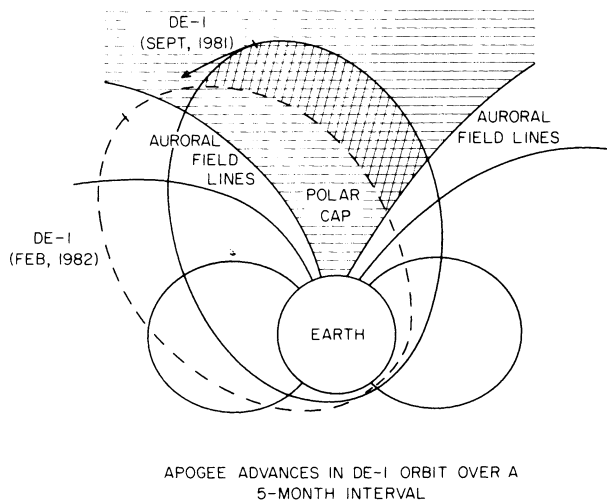APOGEE ADVANCES IN DE-1 ORBIT OVER A
5-MONTH INTERVAL

Fig. 1. The change in the orientation of the DE 1 orbit from September 1981 to February 1982. All density data presented in this study for the 5-month interval, indicated by the crossing shading, are from high-latitude passes over the polar cap region.

the DE 1 orbit in September 1981 and the precession of the apogee over the 5-month period involved in this study, from September 1981 to February 1982. The latitudinal precession of the DE 1 apogee is 108° per year. This precession is responsible both for the variations in the altitude of the spacecraft in the polar cap region and for the variations in the length of time the spacecraft spends in this region. During the 5-month period covered in this study, the geocentric radial distance of DE 1 in the northern polar cap region varied from 2.0 R_E to 4.66 R_E, or 6378 km to 23,343 km above the earth's surface. This altitude range is far below the high altitudes surveyed by the Hawkeye spacecraft and above the low altitudes investigated by the topside sounder satellites and the polar orbiting satellites making in situ density measurements in the polar cap.

DE 1 electron density measurements have been obtained by an analysis of whistler mode wave propagation using electric field spectrum measurements from the plasma wave instrument. The plasma wave instrument (PWI) on Dynamics Explorer 1 has been described in detail in a previous report [see Shawhan et al., 1981]. The instrument is designed to measure ac electric fields over a frequency range of 1 Hz to 2 MHz and an amplitude range of 0.03 μV m^{-1} to 100 mV m^{-1}. Ac magnetic fields and quasi-static electric fields are also measured. The antenna system used to detect electric fields consists of a pair of electric antennas mounted orthogonally to each other. One of these antennas is 9 m long and is oriented parallel to the spin axis, and the other is 200 m long and is oriented perpendicular to the spin axis. Signals from these sensors are processed by two of the PWI receiver systems, the step frequency correlator (SFC) and the low frequency correlator (LFC). The step frequency correlator consists of a correlator and two identical step frequency receivers (SFR) with four frequency bands, each containing 32 frequency steps. The SFC scans a frequency range of 100 Hz to 400 kHz once every 32 s. The low frequency correlator consists of a correlator and two identical spectrum analyzers, each with eight filters. The LFC scans a frequency range of 1.78 Hz to 100 Hz once every 32 s. The resulting electric field amplitude measurements are displayed in frequency-time spectrogram form. Each spectrogram covers a 2-hour time interval and spans a frequency range of 1.78 Hz to 400 kHz.

2. Method of Analysis

Electric field spectrograms obtained from the electric field amplitude measurements of the PWI illustrate features of the various modes of plasma waves observed by DE 1 for frequencies in the vicinity of the electron gyrofrequency and the electron plasma frequency. Four plasma wave modes are predicted by cold plasma theory in this frequency range [Stix, 1962]. Of these modes, the whistler mode, the Z mode, and the R-X mode have been associated with electromagnetic plasma wave emissions found in the auroral zone and polar cap region [Gurnett et al., 1983]. Broadband electromagnetic emissions propagating below the electron gyrofrequency in the auroral zone (where $f_g < f_p$) are called auroral hiss. These emissions are believed to be propagating in the whistler mode [Gurnett et al., 1983] because this is the only electromagnetic plasma wave mode propagating in this frequency range. Auroral hiss is generated by low-energy (100 eV to 10 keV) electrons moving upward along auroral field lines from a region of electron acceleration between 1.7 R_E and 1.9 R_E [Lin et al., 1983]. Intense, high-frequency emissions called auroral kilometric radiation (AKR) have also been identified on the PWI electric field spectrograms. This radiation is generated along auroral field lines between 2 R_E and 4 R_E [Gurnett, 1974; Gallagher and Gurnett, 1979] and escapes from the earth's magnetosphere. Recent polarization measurements of AKR by Shawhan and Gurnett [1982] have determined that the dominant component of AKR is right-hand polarized and the radiation propagates in the free space R-X mode. Broadband Z mode radiation has been identified in the auroral zone by Calvert [1981] and Gurnett et al. [1983].

A typical example of an electric field spectrogram illustrating these various wave modes is shown in Figure 2. The trajectory of the spacecraft in a magnetic meridian plane is shown in the lower left corner of the spectrogram. In this case, the spacecraft is approaching the nightside auroral region from a radial distance of 4.2 R_E and 79° magnetic latitude and entering the auroral zone at 54° magnetic latitude and a radial distance of 2.8 R_E. The intense emissions in the high-frequency range are auroral kilometric radiation. The apparent lower frequency cutoff of auroral kilometric radiation is an instrumentation effect; the low-frequency cutoff of the step frequency receivers' fourth frequency band is located at 58 kHz. The emissions in the 15–60 kHz range are Z mode radiation, electromagnetic emissions with a characteristic upper frequency cutoff located at the upper hybrid resonance frequency [Gurnett et al., 1983]. In this spectrogram, the Z mode radiation exhibits a sharply defined upper frequency cutoff at the electron gyrofrequency on the poleward side of the auroral zone. In this region of low electron densities, the electron plasma frequency is much lower than the local electron gyrofrequency. Under these circumstances, the upper hybrid resonance frequency is approximately equal to the local electron gyrofrequency and the latter becomes the upper frequency cutoff for the Z mode.

The intense emissions below 20 kHz which spread out from the auroral region toward the pole are auroral hiss emissions. Auroral hiss is commonly observed between 10 Hz and 100 kHz. Figure 2 illustrates the funnel-shaped lower frequency cutoff of auroral hiss emissions in the auroral zone, a feature that is frequently but not always observed at the altitude of the DE 1 orbit [Gurnett et al., 1983]. Auroral hiss is not confined to the auroral zone but spreads out over a wide range of latitudes both poleward and equatorward of the au-
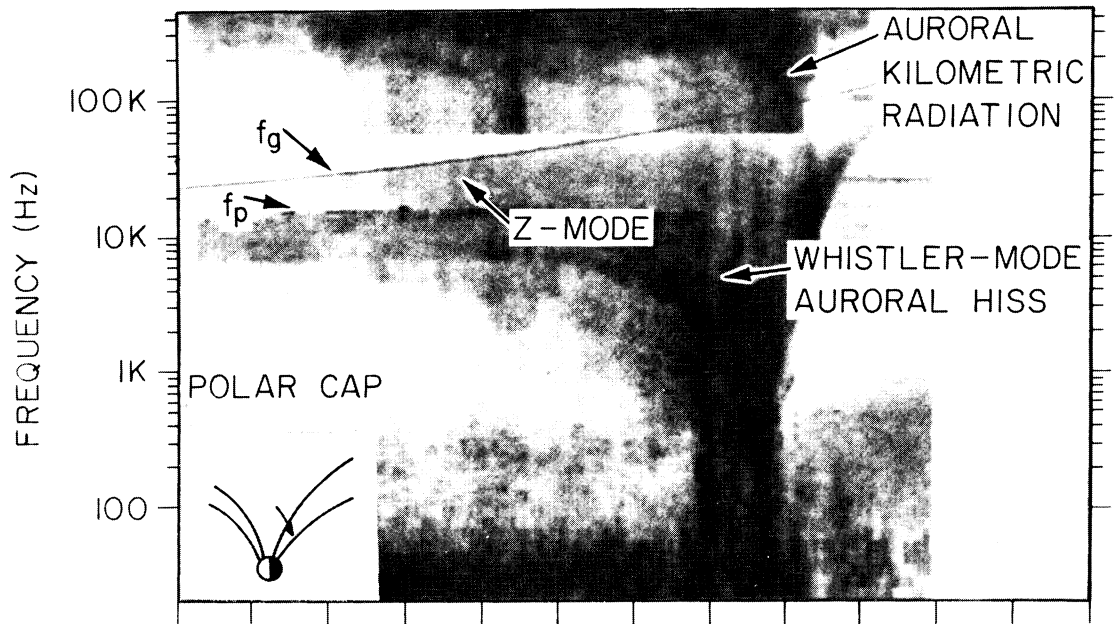
Fig. 2. A representative spectrogram of electric field amplitude measurements illustrating the various plasma wave emissions found in the polar cap region near the electron gyrofrequency and plasma frequency.

roral zone. Auroral hiss emissions are also found in the dayside polar cusp and sometimes exhibit a latitudinal asymmetry in the direction of the pole (see Figure 3), resulting in a nearly continuous band of emissions over the polar cap region (see Figures 4 and 5).

Since auroral hiss is a whistler mode emission, this radiation has a characteristic upper frequency cutoff at either the electron gyrofrequency or the electron plasma frequency, whichever is smaller [Stix, 1962; Chen, 1974]. In the polar cap region, the electron plasma frequency is generally much smaller than the electron gyrofrequency. The electron plasma frequency then gives the upper frequency cutoff for the whistler mode. In Figure 2, the plasma frequency cutoff is well defined and varies smoothly from 16 to 19 kHz. It distinguishes the auroral hiss emissions below from the Z mode radiation above.

Spectrograms, such as the one in Figure 2, are constructed from the digitized data output of the step frequency receivers. To trace the plasma frequency cutoff, the digitized data are displayed on a video monitor in spectrogram form. A manually controlled cursor is then used to trace the plasma frequency cutoff on the spectrogram, and a frequency value is recorded for each sweep of the step frequency receiver (every 32 s). In addition, orbit parameters of the spacecraft, such as magnetic latitude and radial distance, are recorded for each 32-s time interval.

For spectrograms in which the upper frequency cutoff is not clearly defined, contrast enhancement techniques are employed to accent the plasma frequency cutoff and minimize

background noise and Z mode radiation. A 16-point sliding grey scale provides the capability of enhancing the intensity of segments of the frequency range by raising the minimum intensity levels above the maximum intensity of the background noise and lowering the maximum intensity levels displayed on the monitor screen. The remaining narrower intensity range is spanned by 16 shades from white (lowest intensity) to black (highest intensity). Such contrast enhancement techniques are necessary, since an accurate determination of the electron number density depends on the measurement of a well-defined plasma frequency cutoff.

The combined use of contrast enhancement techniques and tracing the frequency cutoff with a cursor permits the determination of the frequency cutoff to a high degree of accuracy. The top three SFR frequency bands (900 Hz to 400 kHz) are divided into 96 frequency steps. The cursor can locate the frequency cutoff within one frequency step. At 10 kHz, a typical frequency cutoff value, the frequency cutoff can be determined within ± 600 Hz, corresponding to an uncertainty in the calculated number density of $\pm 12\%$. This uncertainty is negligible compared to the observed spread in density values due to diurnal and latitudinal variations, as well as anticipated large-scale variations due to magnetic activity and solar effects.

An additional source of error comes from the identification of the cutoff frequency with the electron plasma frequency. Hot plasma effects such as cyclotron damping and Landau damping can cause the whistler mode wave to cut off at frequencies below the electron plasma frequency. These effects,
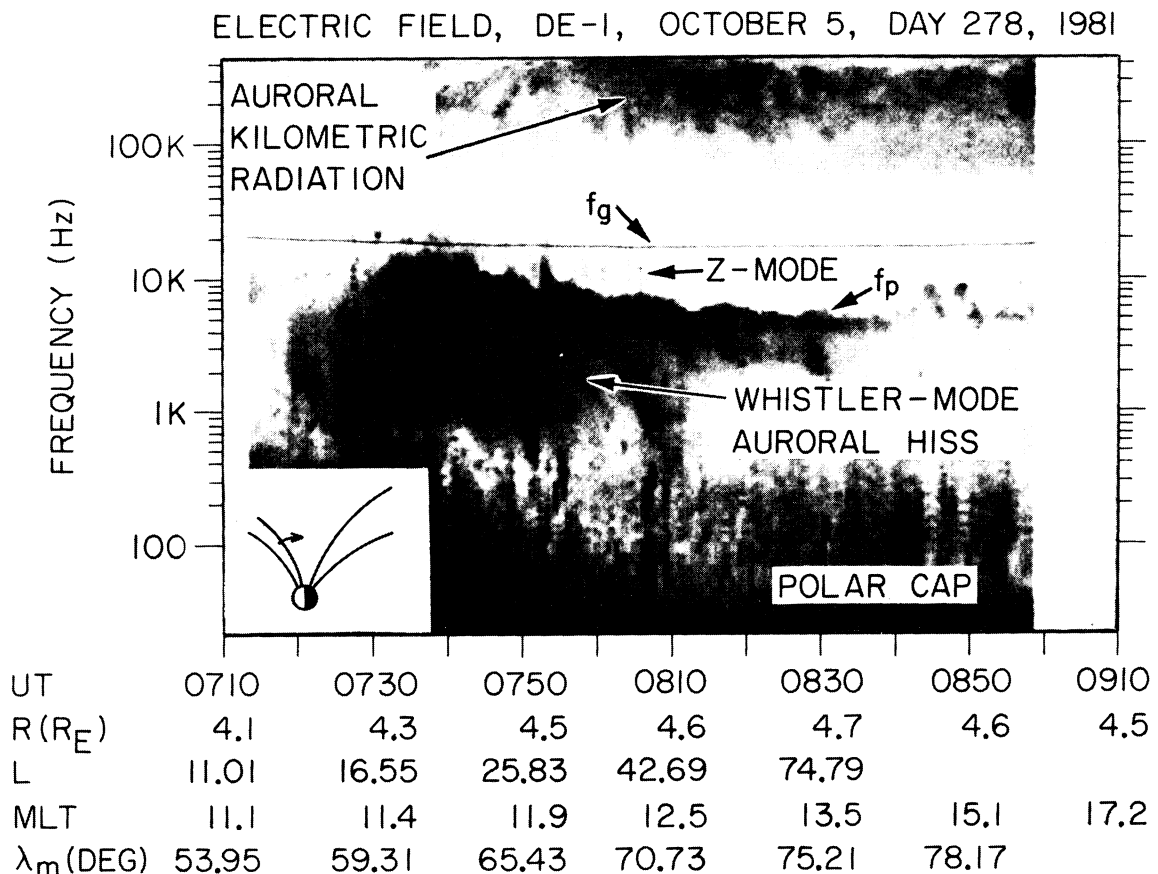
Fig. 3. An electric field spectrogram of a polar cusp crossing in early October. Irregularities in the density profile are indicated by sudden increases in f_p at 0752 UT and at 0845–0850 UT as the satellite nears the pole.

however, are expected to be small. Because of the small wave normal angle of the whistler mode at resonance and the subsequently high index of refraction required for Landau damping, this effect will only be significant in a narrow band of frequencies just below the plasma frequency. Only particles with resonant frequencies in this band will interact with the wave. For frequencies in the range of $f_p \pm 0.2$ kHz, the Landau damping effect would imply an error in the calculated number density of approximately 4% at $f_p = 10$ kHz. Cyclotron damping will have a significant effect on the cutoff frequency only in a region near the electron gyrofrequency. A statistical comparison of the electron gyrofrequency and the observed cutoff frequency on the electric field spectrograms indicates that the cutoff frequency was equal to or greater than 0.9 f_g for only 2% of all data points in this study (see section 4). Consequently, if errors occur due to cyclotron damping they occur in less than 2% of all the density data points. The cyclotron damping effect is negligible below 3.5 R_E and is expected to be smaller than the Landau damping effect at all radial distances.

The method of determining the electron number density from the plasma frequency cutoff has certain inherent limitations. The plasma frequency can be determined with the aforementioned accuracy only for those spectrograms where auroral hiss is present and where the cutoff is reasonably well-defined. Of the more than 750 electric field spectrograms examined in this study, only 40% have auroral hiss with well-defined upper frequency cutoffs for a significant fraction of the 2-hour time interval of the spectrogram. The quality of the upper frequency cutoff on these spectrograms varies with the intensity of the whistler mode radiation as well as with the

intensity of the background noise and the other plasma wave modes (particularly the Z mode) propagating near the upper frequency cutoff. The quality of the frequency cutoff tends to improve toward the lower polar latitudes. Few well-defined frequency cutoffs could be found for magnetic latitudes above 85°. The intensity of auroral hiss emissions propagating into the polar cap from lower auroral latitudes diminishes with increasing latitude, thereby making it difficult to find suitable events at high latitudes over the polar cap. Frequently, at high latitudes, auroral hiss emissions could not be distinguished from the background noise.

3. REPRESENTATIVE ELECTRIC FIELD SPECTROGRAMS

To provide a feeling for the type of data used and the difficulties encountered, five representative passes have been selected for discussion. These passes were selected to illustrate a range of conditions, varying from very smooth, well-defined electron density profiles to highly irregular profiles with large variations on a short time scale.

3.1. Day 278, 1981

The spectrogram for this pass is shown in Figure 3. The electron density profile is smooth and well-defined up until 0840 UT as the satellite nears the pole. The spectrogram is from early October 1981, when the satellite's apogee had precessed about 15° to the dayside of the pole. The panel in the lower left hand corner of the spectrogram indicates the satellite's trajectory. DE 1 is emerging from the dayside polar cusp at 4.3 R_E with a magnetic latitude of 59° and approaching the pole at 4.6 R_E and 78° magnetic latitude at 0858 UT, where

there is a data gap. Intense AKR is again evident above 100 kHz and Z mode radiation, less intense than it was in Figure 2, is found between 10 kHz and 20 kHz at 0755 UT. The auroral hiss emissions are latitudinally asymmetric, spreading out over the polar cap region in the direction of the pole. However, the funnel-shaped lower frequency cutoff of the auroral hiss in the auroral zone is not evident in this spectrogram. Below 78° magnetic latitude, the electron plasma frequency is smoothly varying, decreasing with increasing radial distance. Exceptions are the sharp spike in the plasma frequency cutoff at 0752 UT and several spikes after 0845 UT, indicating a sudden increase in the electron number density by more than a factor of 2. After about 0840 UT, the auroral hiss becomes weak and the upper cutoff becomes irregular and difficult to identify.

3.2. Day 047, 1982

The two spectrograms in Figures 4 and 5 were chosen to illustrate one continuous pass of DE 1 over the polar cap. This pass occurred in mid-February of 1982 when the spacecraft apogee had precessed into the nightside auroral zone. In Figure 4, the spacecraft is in and emerging from the nightside auroral zone as illustrated by the panel in the bottom left-hand corner of the spectrogram. It passes through apogee at approximately 0350 UT and emerges from the auroral zone shortly after 0405 UT, with a range in magnetic latitude of 34° to 69°. An abrupt drop in the plasma density is evident in the auroral zone from about 0400 to 0405 UT. This density depletion is believed to correspond to the auroral plasma cavity discussed by *Calvert* [1981]. In the polar cap region, the

plasma frequency cutoff of the whistler mode radiation is sharply defined and constant at approximately 10 kHz. The Z mode radiation above the auroral hiss is less intense and again exhibits a sharp upper frequency cutoff at the electron gyrofrequency.

The spectrogram in Figure 5 is a continuation of the 2-hour spectrogram in Figure 4. The spacecraft is in the northern polar cap region for most of this time interval, passing over the pole at approximately 0600 UT. The vertical white lines on the spectrogram indicate short data gaps. The radial distance of the spacecraft for this spectrogram varies from 4.4 R_E at a magnetic latitude of 62° on the nightside of the pole to 1.8 R_E at a magnetic latitude of 44° on the dayside of the pole. The spacecraft enters the polar cusp at approximately 0640 UT, as indicated by the onset of broadband auroral hiss emissions at that time. The plasma frequency cutoff in Figure 5 is again sharply defined and is generally constant at about 16 kHz before the spacecraft crosses the pole. However, there is an abrupt 12% decrease in magnitude at a magnetic latitude of 84° on the dayside of the pole (at 0604 UT) and a steady increase in the plasma frequency after 0625 UT with decreasing radial distance. Generally, though, the plasma frequency in Figures 4 and 5 exhibits few variations on a short time scale, and the resulting electron density profile for this orbital pass is smoothly varying.

3.3 Day 046, 1982

However, the plasma frequency is not smoothly varying for the orbital pass which immediately precedes the pass illustrated in Figures 4 and 5. In Figure 6 the spacecraft is in the
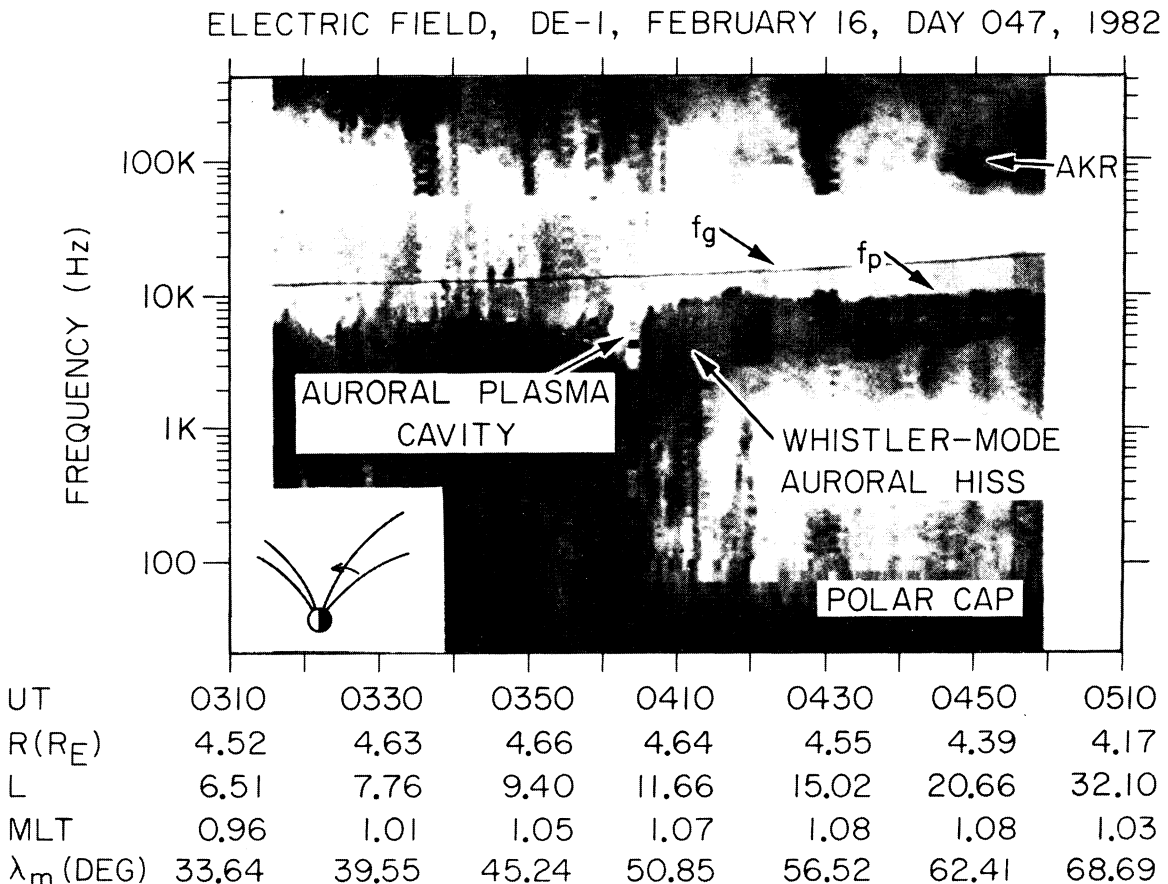

UT	0310	0330	0350	0410	0430	0450	0510
R(R_E)	4.52	4.63	4.66	4.64	4.55	4.39	4.17
L	6.51	7.76	9.40	11.66	15.02	20.66	32.10
MLT	0.96	1.01	1.05	1.07	1.08	1.08	1.03
λ_m (DEG)	33.64	39.55	45.24	50.85	56.52	62.41	68.69

Fig. 4. A nightside crossing of the auroral field lines in mid-February illustrating a depletion in electron densities at $\lambda_m \simeq 50°$ [*Calvert*, 1981] and a smooth density profile inside the polar cap region.

ELECTRIC FIELD, DE-I, FEBRUARY 16, DAY 047, 1982

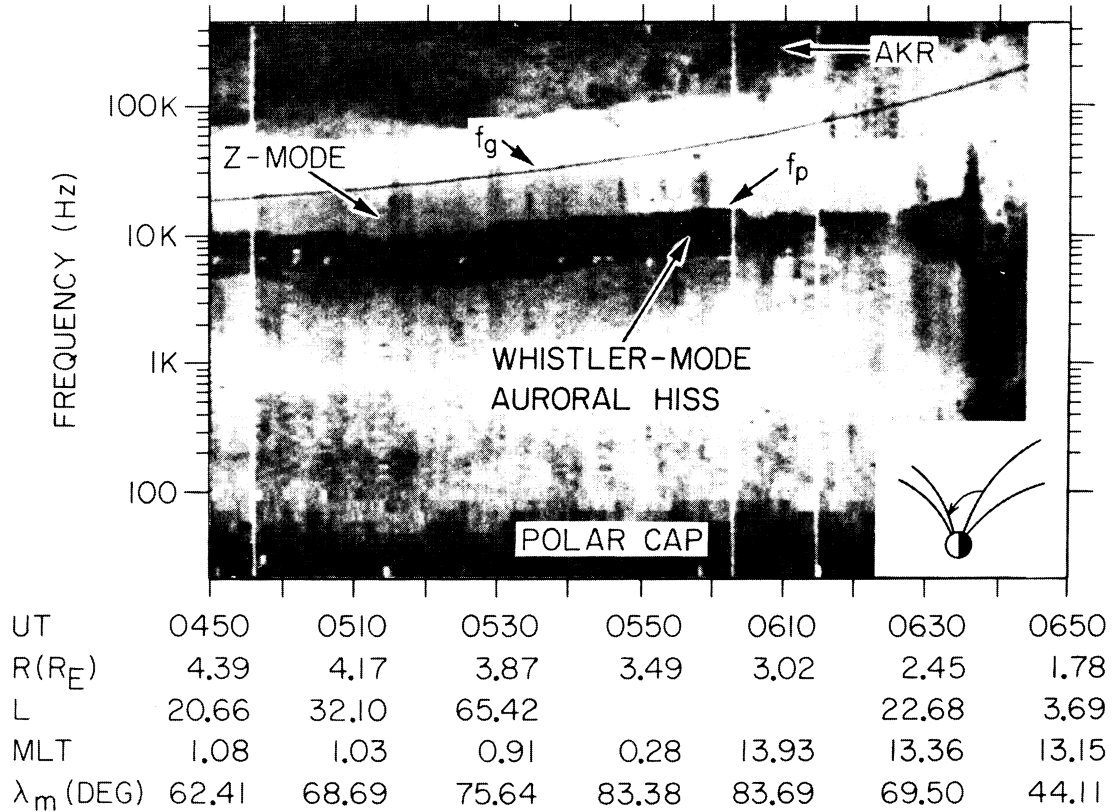| UT	0450	0510	0530	0550	0610	0630	0650
R(R$_E$)	4.39	4.17	3.87	3.49	3.02	2.45	1.78
L	20.66	32.10	65.42			22.68	3.69
MLT	1.08	1.03	0.91	0.28	13.93	13.36	13.15
λ_m (DEG)	62.41	68.69	75.64	83.38	83.69	69.50	44.11

Fig. 5. A continuation of the same polar pass illustrated in Figure 4. The density profile is smoothly varying over the entire polar cap region.

same region of the polar magnetosphere as it is in Figures 4 and 5 but 6 hours earlier. As indicated in the panel in the lower right hand corner, DE 1 is emerging from the nightside auroral zone into the northern polar cap region. In this 2-hour interval, the radial distance of the spacecraft varies from 4.4 R_E at a magnetic latitude of 47 on the nightside of the pole to 1.8 R_E at a magnetic latitude of 51° on the dayside of the pole.

We believe that the radiation seen below 40 kHz at high magnetic latitudes in Figure 6 is electromagnetic. The radiation propagates at frequencies below the electron plasma frequency in a region of the polar magnetosphere where $f_p \ll f_g$. Whistler mode radiation is the only electromagnetic plasma wave mode that can propagate in this frequency range. This whistler mode radiation, however, is not the usual type of auroral hiss associated with the auroral zone, since it is believed to be generated at high magnetic latitudes poleward of the auroral field lines. This radiation may be associated with the polar cap aurora or other auroralike processes observed over the polar cap [Frank et al., 1982].

Since the radiation is whistler mode radiation, the upper frequency cutoff visible in Figure 6 is the electron plasma frequency. Unlike the plasma frequency cutoff in Figures 4 and 5, the plasma frequency cutoff in Figure 6 is highly variable on time scales of 8 min to less than 1 min, indicating variations in the electron number density of an order of magnitude or more on spatial scales of 50–1400 km.

3.4. Day 039, 1982

The variability in the character of the electron density profile between successive passes of the spacecraft is again illustrated in Figures 7 and 8. The spectrograms in these figures

are from successive passes of the spacecraft, emerging from the nightside auroral zone in early February 1982. In Figure 7, the spacecraft exits the auroral zone at 0400 UT at a radial distance of 4.6 R_E and a magnetic latitude of approximately 45° and passes through apogee in the polar cap region about 10 min later. In this spectrogram, the electron plasma frequency varies smoothly between 9 kHz and 13 kHz with few abrupt changes on a short time scale, indicating changes in the electron number density by a factor of 2 or less.

On the following pass (Figure 8), the spacecraft emerges from the nightside auroral zone at 1140 UT (approximately 7.5 hours later) at a radial distance of 4.5 R_E and a magnetic latitude of 50. The radial distance of the spacecraft in the polar cap region for this pass varies from 4.5 R_E at a magnetic of 50° to 3 R_E at a magnetic latitude of 78° on the nightside of the pole, very similar to the preceding pass. However, unlike the preceding pass, the electron plasma frequency cutoff is not smoothly varying. There is a general tendency for the plasma frequency to increase in magnitude with decreasing radial distance as the spacecraft near the pole, as it did in Figure 7. But more striking are the large variations in the magnitude of the plasma frequency on time scales of 5 min or less, indicating variations in the electron number density up to 1 order of magnitude on spatial scales of less than 700 km. The electron density profile for this pass is not as smoothly varying as it was in Figure 7.

4. The Electron Density Profile

To obtain the electron density profile in the northern polar cap region, the electron plasma frequency was numerically
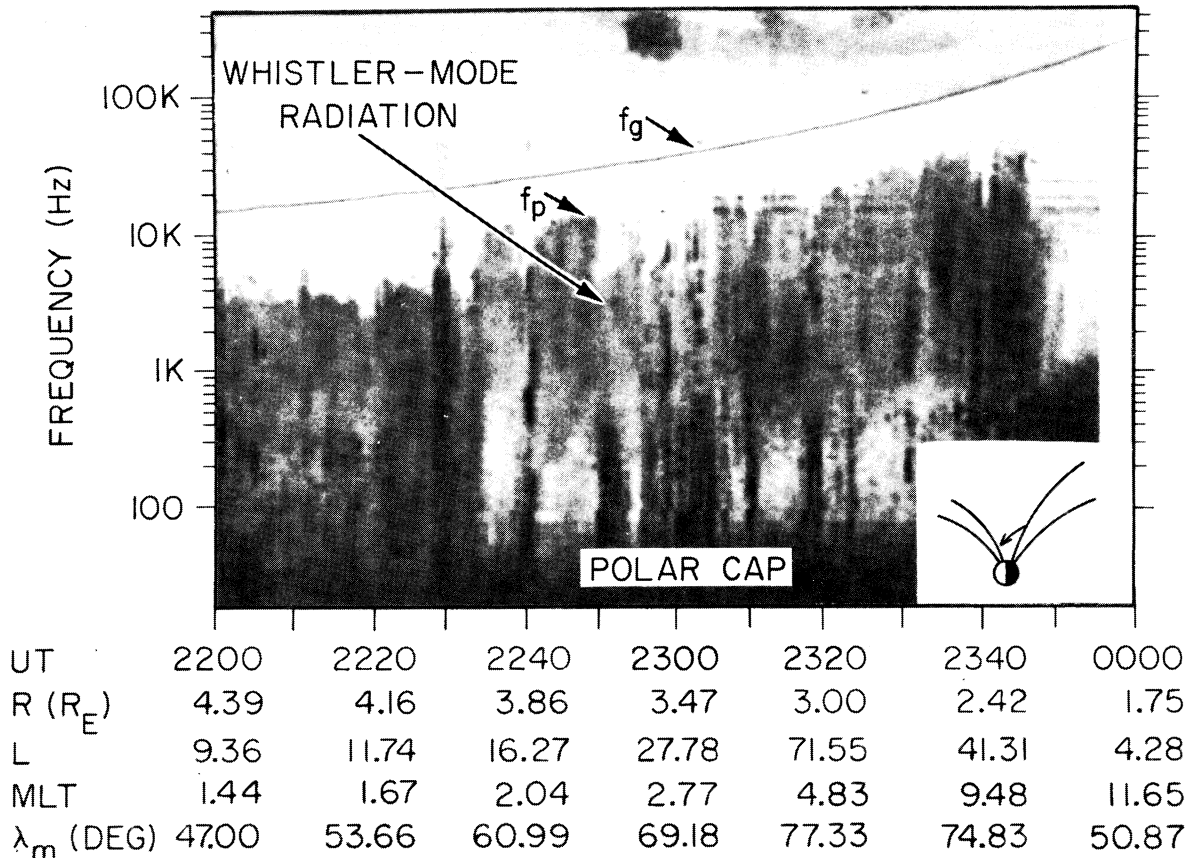
Fig. 6. A spectrogram illustrating the time variability of the density profile. This pass preceded the pass illustrated in Figures 4 and 5 by just 6 hours for the same region of the polar magnetosphere. The density profile is highly variable on very short spatial scales.

determined from the analysis of nearly one hundred 2-hour spectrograms over the polar cap, selected from the 5-month time interval from September 1981 to February 1982. This interval was characterized by relatively high magnetic activity ($\overline{kp} \simeq 3$). The electron number density was calculated from the plasma frequency by using the relation $n_e = (f_p/9)^2$, where n_e is in cm^{-3} and f_p is in kHz. Figure 9 is a semilog plot of the calculated electron number density as a function of radial distance. This plot shows that a wide scatter exists in the electron density for a given radial distance. This scatter is not unexpected, since the examination of individual passes shows large variations from orbit to orbit as well as substantial variations on individual passes. The scatter plot also combines data over a wide range of magnetic latitudes, so that some of the scatter could be due to variations of the latitudinal position of the spacecraft within the polar cap. Despite the wide spread in the electron density values at a given radial distance the electron density is clearly seen to decrease with increasing radial distance, as would be expected.

The sharply defined upper density cutoff evident in Figure 9 from about 3.5 to 4.6 R_E corresponds to the electron gyrofrequency. This upper cutoff occurs because the electron number densities can be determined from the whistler mode cutoff frequency only when the electron plasma frequency is lower than the electron gyrofrequency. When the electron plasma frequency exceeds the gyrofrequency, the electron density calculated from the cutoff frequency (now the electron gyrofrequency) merely represents a lower limit on the actual

electron density. A statistical tabulation of the data points for which the cutoff frequency was greater than 90% of the electron gyrofrequency indicated that the electron gyrofrequency contaminated the calculation of electron densities in less than 1% of the cases below 3.5 R_E, increasing to about 3.6% of the cases for radial distances above 4.25 R_E. A total of approximately 2% of all density values are affected.

To further explore the relationship between electron density and radial distance and to determine the spread in number density values for a given altitude, the radial range was divided into radial increments of 0.25 R_E and the median value of the electron number density was computed for each radial increment. All cutoff frequencies were used in calculating the median values, even when the cutoff is determined by the gyrofrequency. Median values were chosen, rather than average values, to eliminate the effect of plasma frequencies greater than the gyrofrequency. Since the medians, are in all cases, well below the gyrofrequency, median values are not affected by the gyrofrequency cutoff. Figure 10 is a log-log plot of the median electron number density as a function of radial distance. The error bars indicate quartiles, which show the spread in 25% of the data on either side of the median values. The median number densities range from 35.2 ± 8.5 cm^{-3} at 2.1 R_E to 0.99 ± 0.51 cm^{-3} at 4.66 R_E. Variations up to a factor of 4 occur from these median values. As can be seen from Figure 10, a straight line provides a good fit through the median points, thereby suggesting a power law relationship between the electron density and the radial dis-
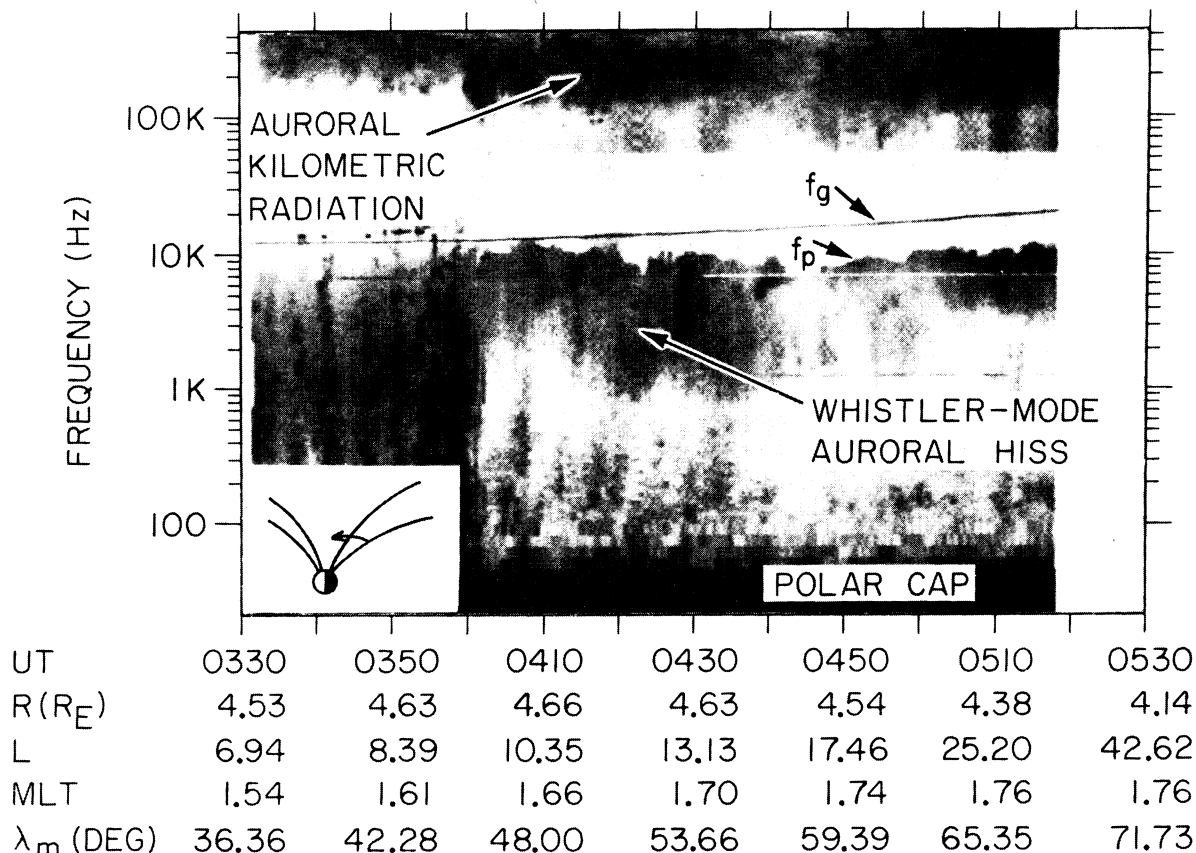
ELECTRIC FIELD, DE-I, FEBRUARY 8, DAY 039, 1982

UT	0330	0350	0410	0430	0450	0510	0530
R (R_E)	4.53	4.63	4.66	4.63	4.54	4.38	4.14
L	6.94	8.39	10.35	13.13	17.46	25.20	42.62
MLT	1.54	1.61	1.66	1.70	1.74	1.76	1.76
λ_m (DEG)	36.36	42.28	48.00	53.66	59.39	65.35	71.73

Fig. 7. Another nightside crossing of the auroral field lines in early February. Changes in the cutoff frequency for this pass indicate small variations in the number density by a factor of 2 or less.

tance. The slope of the best fit line through the points indicates a power law exponent of -3.85 ± 0.32.

5. COMPARISON OF THE DENSITY PROFILES WITH THEORETICAL MODELS

In the high-density, low-latitude region of the earth's magnetosphere, plasma is confined on closed magnetic field lines and exists in a state of near-diffusive equilibrium [Dessler and Michel, 1966; Dungey, 1961]. In this region, diffusive equilibrium solutions can be obtained assuming a Maxwellian velocity distribution and a collision-dominated plasma [Bauer, 1969]. However, at high geomagnetic latitudes the magnetic field lines are open to interplanetary space. In this region the boundary plasma pressure is very low, and an outward flow of ionospheric ions results [Banks and Holzer, 1968, 1969b]. The outward flux of predominantly light ions has been called the polar wind [Axford, 1968]. Because the plasma escapes freely from the magnetosphere the electron density drops to very low values at all polar latitudes. At low polar altitudes, convection processes in the F region also contribute to a substantial depletion of ionospheric plasma. Evidence of significant plasma depletions at low altitudes in the polar region has been given by Hagg [1967] and Timleck and Nelms [1969].

The existence of an upward, field-aligned flux of protons, predicted by the polar wind theory, was confirmed by Explorer 31 and ISIS 2. The ion mass spectrometers on these satellites detected an upward proton flux in the low plasma

density region of the polar cap above 1000 km [Hoffman, 1969; Hoffman and Dodson, 1980]. At the higher altitudes of the DE 1 orbit, the retarding ion mass spectrometer and the energetic ion composition spectrometer have both detected a similar flux of lighter ions (H^+ and He^+) in the polar cap region [Chappell et al., 1982a; Shelley et al., 1982]. A significant flux of N^+ ions [Chappell et al., 1982b] has also been detected, and recent measurements have discovered a peak in the flux of the O^+ ion [Shelley et al., 1982] which appears to be associated with periods of increased magnetic activity ($kp > 5$) (J. H. Waite, personal communication, 1983).

The escape of ions from the polar cap region is constrained by the continuity equation which, for a specific ion species, can be written

$$(\partial n_i/\partial t) + \nabla \cdot (n_i \mathbf{U}_i) = q_i - l_i \qquad (1)$$

where n_i is the ion number density, $\mathbf{U}_i$ is the ion flow velocity, q_i is the ion production rate, and l_i is the ion loss rate. The form of the continuity equation can be greatly simplified by adopting three assumptions pertaining to the high-altitude polar magnetosphere: steady state conditions, negligible ion loss and production, and a negligible divergence in the perpendicular ion flux. The assumption of negligible ion loss and production is justified by the low neutral particle densities encountered in the polar magnetosphere at radial distances greater than 2 R_E. The assumption of a negligible divergence of the perpendicular ion flux is reasonable, as a first-order approximation, at high polar altitudes where the radial

ELECTRIC FIELD, DE-I, FEBRUARY 8, DAY 039, 1982
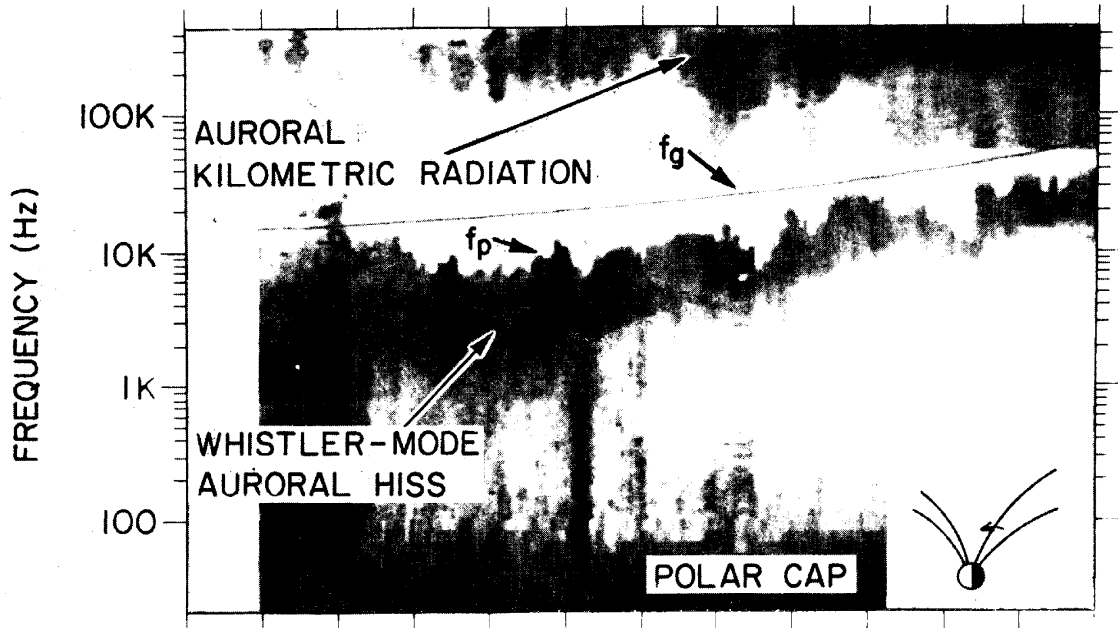
UT	1120	1140	1200	1220	1240	1300	1320
R (R_E)	4.63	4.54	4.38	4.16	3.85	3.47	2.99
L	9.41	10.84	12.82	15.89	21.74	36.31	85.75
MLT	0.71	0.55	0.37	0.12	23.76	23.09	21.30
λ_m (DEG)	45.68	49.89	54.35	59.24	64.81	71.27	77.98

Fig. 8. This pass follows the pass illustrated in Figure 7 by 7.5 hours for the region of the polar magnetosphere just poleward of the nightside auroral zone. The density profile is highly irregular with fluctuations up to an order of magnitude on spatial scales of less than 700 km.

plasma outflow is dominant. Although steady state conditions do not exist at all times in the polar magnetosphere, steady state is a justifiable first-order approximation when the density measurements are time-averaged over several months, as we have done. With these approximations, the continuity equation for a simple radial outflow model requires that

$$n_i u_i A = \text{const} \tag{2}$$

where u_i is the ion flow velocity parallel to the magnetic field and A is the cross-sectional area of the flux tube at a given radial distance. The cross-sectional area of the flux tube can be shown to be proportional to the cube of the radial distance by the conservation of magnetic flux and the dipole approximation for the magnetic field intensity in the polar cap region ($B \propto R^{-3}$). Thus the continuity equation for the steady state radial outflow of ions along magnetic field lines, neglecting ion loss and production and the perpendicular ion flux, predicts that

$$n_i \propto u_i^{-1} R^{-3} \tag{3}$$

where $A \propto R^3$ has been substituted for the cross-sectional area of the flux tube in the continuity equation.

The condition of electrical neutrality in the polar cap region requires that

$$n_e = \sum_i Z_i n_i \tag{4}$$

where Z_i is the charge state of the individual ion species. Since one singly charged ion species is expected to dominate at large radial distances (H^+ in the model developed by Banks and Holzer), the electron density is controlled by that species. Assuming therefore that $n_e \approx n_i$, it follows that

$$n_e \propto u^{-1} R^{-3} \tag{5}$$

where u is the plasma flow velocity along the magnetic field line. A constant plasma flow velocity would place an upper limit on the exponent of a power law distribution of -3.

In practice, one expects the steady state flow velocity to increase with increasing radial distance because of the pressure gradient between the ionosphere and the magnetotail. This increase in the flow velocity with increasing radial distance can be seen in the calculations of Banks and Holzer [1969a, b] and of Schunk and Watkins [1981, 1982]. Thus the exponent greater than 3 in Figure 10 is consistent with the expected relationships of radial distance with flow velocity and cross-sectional area in the polar cap region. It is reasonable to expect that $n_e \propto R^{-\gamma}$, where $\gamma > 3$, if a valid power law relationship exists between electron number density and radial distance. Our best data fit in Figure 10, $n_e \propto R^{-3.85 \pm 0.32}$, indicates that the plasma flow velocity increase as $R^{0.85 \pm 0.32}$ (i.e., approximately linearly with radial distance).

An outward flux of light ions and electrons is expected to occur in the polar cap region [Axford, 1968; Banks and Holzer, 1968]. However, the newly discovered dominance of
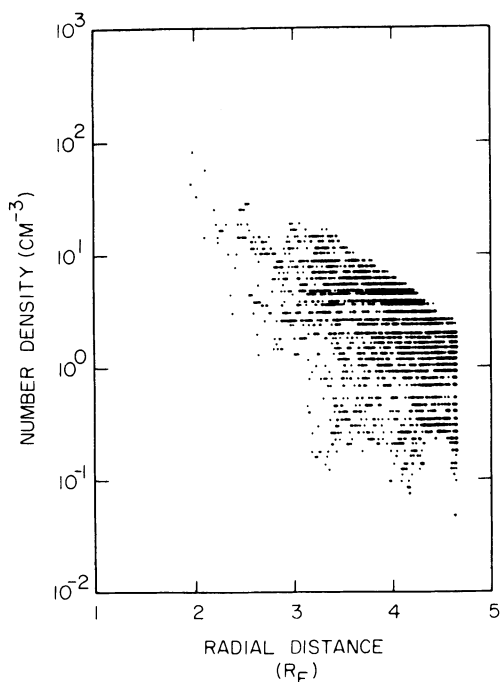
Fig. 9. A scatter plot of electron density as a function of radial distance. The large scatter in the data is mainly due to temporal variations in the electron density. The sharp upper cutoff evident from about 3.5 to 4.6 R_E is caused by the whistler mode propagation cutoff at the electron gyrofrequency.

the oxygen ion for some DE 1 polar passes was unexpected [Shelley et al., 1982]. The classic polar wind theory predicted a large flux of lighter ions along open magnetic field lines at high latitudes and a negligible loss of heavy ions. Calculations showed that the loss of light ions from the topside polar ionosphere would result in a dominance of O^+ ions up to an altitude of 4000 km to 7500 km. Above this altitude a substantial, though rapidly diminishing, upward O^+ flux would exist to support the dominant H^+ flux through charge-exchange reactions.

In their theoretical study of multicomponent plasma transport at high geomagnetic latitudes, Banks and Holzer [1969b] derived a set of solutions to the standard hydrodynamic transport equations for various neutral atmosphere models and a range of isotropic, equal electron and ion temperatures. At an altitude of 7000 km (2.18 R_E), their predicted electron densities ranged from approximately 80 cm^{-3} to nearly 1000 cm^{-3}. These densities exceed our observed densities at 2.25 R_E by a factor of 5–50.

Banks and Holzer [1969b] also derived a set of predicted ion densities for different neutral atmosphere temperatures and a range of equal electron and ion temperatures. Predicted O^+ densities were found to vary from 10 cm^{-3} to 200 cm^{-3} and H^+ densities from 90 cm^{-3} to 120 cm^{-3} at 7000 km. The altitude of the transition from dominant O^+ at low altitudes to dominant H^+ at higher altitudes was found to vary between 4000 km and 7500 km, depending on the initial concentration of hydrogen in the neutral atmosphere model.

When electron and ion temperatures were allowed to vary individually and anisotropic temperature distributions were included in the analysis of high-latitude plasma transport, the predicted ion density profiles were altered and the transition to a dominance of the H^+ ion was discovered to occur at even

lower altitudes. In 1982, Schunk and Watkins [1982] developed a set of steady state solutions for the high-latitude plasma flow in the altitude range of 1500–12,000 km. Their solutions were derived from the 13-moment system of transport equations for a range of lower boundary conditions which included the H^+ drift velocity, electron and H^+ temperatures and temperature gradients, and ion number densities at 1500 km.

Schunk and Watkins [1982] published ion density predictions both for supersonic ($M > 1$) and subsonic ($M < 1$) H^+ outflows where the Mach number M refers to the ratio of ion flow velocity to the thermal velocity. The 13-moment transport equations predict a significant electron temperature anisotropy ($T_{e\perp} > T_{e\parallel}$) for the supersonic H^+ outflow and an isotropic electron temperature distribution at this altitude range for a subsonic flow. Both sets of ion density predictions are presented in Figure 11 for two lower boundary electron temperature gradients ($\nabla T_e = 0.1°K$ km^{-1}, $\nabla T_e = 1°K$ km^{-1}). As the boundary electron temperature gradient increases, the solutions for the supersonic H^+ outflow show a decrease in the hydrogen ion density and a slight increase in the oxygen ion density. As required by charge neutrality the sum of the two highest ion densities (H^+ and O^+) predicted by these steady state solutions to the plasma transport equations for supersonic H^+ outflow is within $\pm 25\%$ of the median electron density values observed by DE 1 above 2.5 R_E. Predicted ion densities for subsonic H^+ outflow, on the other hand, are much higher at 2 R_E than our data would suggest and the ion density profile drops off with increasing radial distance much more slowly than our measurements indicate.

Recent measurements by the DE 1 high altitude plasma instrument have established the existence of a low energy, field-aligned, supersonic ion flux in the polar cap and a conic component of the ion flux due to the perpendicular heating of
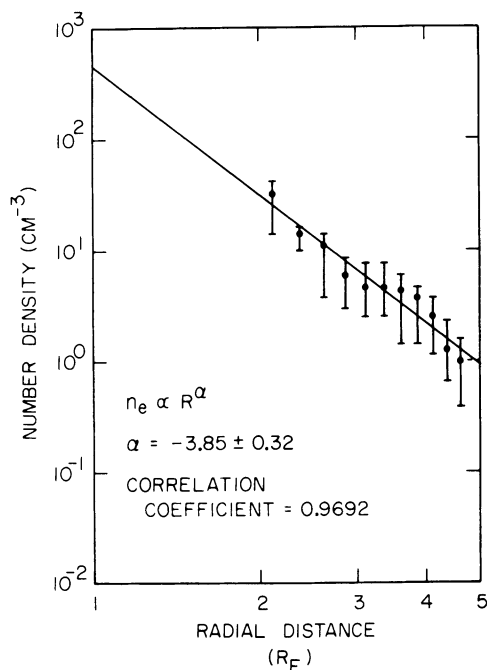

Fig. 10. A log-log plot of median number densities as a function of radial distance. The best line fit through these points indicates a power law distribution for electron densities in the polar cap: $n_e \propto R^{-3.85}$.
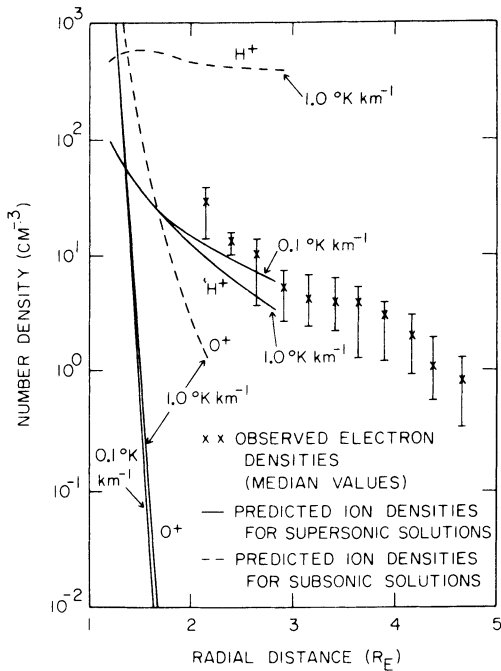
Fig. 11. Predicted ion densities below 2.8 R_E based on solutions to the 13-moment transport equations [Schunk and Watkins, 1982]. The subsonic outflow solutions correspond to higher H^+ and O^+ densities. These predicted densities exceed the DE 1 measured densities at 2 R_E by more than an order of magnitude. Supersonic outflow solutions correspond to lower H^+ and O^+ densities. An increase in the boundary electron temperature gradient (from $0.1°K$ km^{-1} to $1°K$ km^{-1}) corresponds to a slight increase in the predicted O^+ densities and a larger decrease in the predicted H^+ densities. Both sets of predicted ion densities for the supersonic outflow solutions are within 25% of the median density values observed by DE 1.

the field-aligned component [Gurgiolo and Burch, 1982]. The low-energy, field-aligned ions constitute the classical polar wind as described by Axford, [1968]. These measurements suggest that the subsonic H^+ outflow solutions illustrated in Figure 11 are not appropriate in the polar magnetosphere at the altitude of the DE 1 orbit.

Below 2.5 R_E the slightly lower theoretical ion densities based on the polar wind model, illustrated in Figure 11 for supersonic H^+ outflows, are not unexpected, since they are derived from the steady state solutions to the plasma transport equations. The existence of steady state conditions along polar magnetic field lines is related to the convection of plasma across the polar magnetosphere and to the speed of the magnetic convective cycle [Banks and Holzer, 1969b]. Regions of recently disconnected field lines, where the time delay has not been sufficient to achieve a steady state, can be expected to have higher number densities than regions deep in the polar cap. Thus the number density can be expected to vary with magnetic latitude across the polar cap. A rapid convective speed, which shortens the time interval between the merging and reconnection of magnetic field lines, may be sufficiently great to prevent the plasma from achieving a steady state flow in the polar magnetosphere. Under these circumstances, observed number densities across the polar cap will be generally higher than the number densities predicted by the steady state solutions. Variations in the number density due to changes in the magnetic latitude or disturbances in the magnetic field on small time scales have been minimized in this study by averaging densities over all polar magnetic latitudes

for L shell values greater than 10 at any given radial distance. The resulting density profile is expected to be higher than the predicted steady state densities.

6. COMPARISON OF THE HIGH-ALTITUDE DENSITY PROFILE WITH TOPSIDE SOUNDER MEASUREMENTS

Figure 12 is a log-log plot of the electron number density as a function of radial distance from 1.05 R_E to 4.7 R_E. The electron densities for geocentric distances of 1.05 R_E to 1.47 R_E are median density values calculated from a random sampling of more than 350 high-latitude ($\Lambda \geq 80°$) density profiles derived from the Alouette II and ISIS 1 topside sounder data. Error bars indicate the spread in electron density values for this random sampling of Alouette II profiles (1966–1967) and ISIS 1 profiles (1969). The large density variations are due to latitudinal variations in temperature and ionic composition [Nelms and Lockwood, 1967] as well as convective plasma motion in the F region and variations in solar activity and magnetic field conditions.

An abrupt change in the nature of the Alouette/ISIS density profile occurs at approximately 1000 km (1.16 R_E). This transition indicates a change in the basic processes of ion transport in the lower ionosphere. Below 1000 km, conditions of near diffusive equilibrium combined with an outward flux of plasma at subsonic transport speeds are expected to exist [Bauer, 1969]. A vertical diffusive equilibrium distribution is a good approximation to the Alouette/ISIS density profiles below 1000 km. However, the applicability of the model is
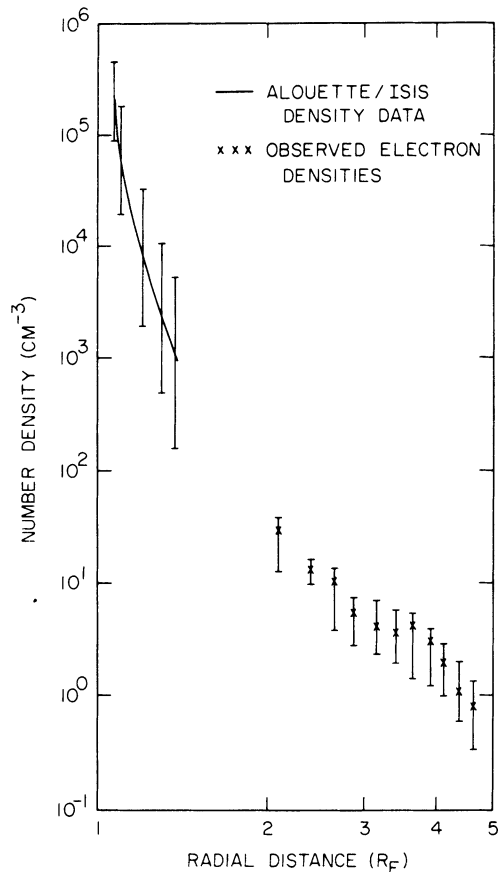

Fig. 12. A log-log plot comparing low-altitude median electron densities obtained from the topside sounder data of Alouette II and ISIS 1 and high-altitude median electron densities obtained from the PWI on DE 1.

limited in the polar cap region by the existence of geomagnetic field lines that open into regions of low plasma pressure in the magnetotail [*Bauer*, 1969]. Such boundary conditions result in an outward plasma flow along the field lines at initially subsonic transport speeds below 1000 km [*Banks and Holzer*, 1969b]. In their steady state solutions of the continuity, momentum and energy hydrodynamic equations for a range of H^+ outflow velocities, *Raitt et al.* [1975] determined that energy losses due to convective plasma motion are significant in determining density distributions between 700 km and 1000 km.

Above 1000 km, a weakening of the charge exchange reaction between molecules and ions and a decrease in ion-ion friction due to rapidly decreasing densities results in an upward plasma flow along magnetic field lines [*Banks and Holzer*, 1969b]. This outward flow, even for low-energy, field-aligned ions, has been found to be supersonic [*Gurgiolo and Burch*, 1982]. The transition to supersonic transport speeds is theoretically expected to occur between 1000 km and 1500 km [*Raitt et al.*, 1975]. However, the assumption of a collisionless plasma, valid at the altitude of the DE 1 orbit, is not valid below 3000 km due to the substantially higher densities in this region. Ion transport processes, consequently, are found to depend in a complicated way on gradients in the plasma parameters and Coulomb collision frequencies [*Schunk and Watkins*, 1981, 1982; *Raitt et al.*, 1975].

In the data gap which occurs between the Alouette/ISIS orbits and the DE 1 orbit (see Figure 12), another transition must occur in order to explain the change in the slope of the density profiles at low and high altitudes. The observed change in the density profile between 1.55 R_E and 2.0 R_E is attributed to the transition from a collision-dominated regime below to a collisionless regime above. In addition to changes in the basic plasma transport processes, transitions in the density profile may also be attributed to changes in the ionic composition and ion acceleration processes in the polar magnetosphere.

The topside sounder data used to derive the median density values observed in Figure 12 are biased toward regions of higher densities (>300 cm^{-3}) by the standard methods of deriving electron densities from topside ionograms [*Nelms and Lockwood*, 1967]. Electron density values for these profiles were calculated indirectly from the extraordinary wave reflection frequency and the gyrofrequency and upper hybrid resonance frequency [*Hagg*, 1967; Alouette II Ionospheric Data from Communications Research Centre in Ottawa, 1966, 1967] for ionograms on which all traces were distinctly visible. This indirect method of deriving density values was employed because the ordinary wave reflection trace at the plasma resonance f_p was not always observed, especially in low-density regions at high latitudes and altitudes where the plasma frequency occasionally fell below the low-frequency limit of the satellite's topside sounder.

In regions of very low electron densities and subsequently low plasma frequencies where $f_p \ll f_g$, the upper hybrid resonance frequency approaches the electron gyrofrequency and the indirect determination of electron density described above could be not used. Interference between the electron gyrofrequency and the upper hybrid resonance results in a difference or modulation frequency that can be determined from the ionograms and used to calculate electron densities below 100 cm^{-3} [*Hagg*, 1967]. The use of a modulation frequency technique to determine low-density values resulted in the dis-

covery of very low electron densities (<100 cm^{-3}) for all polar latitudes ($\lambda_m > 60°$) at radial distances of 1.24–1.47 R_E for selected ionograms on which the extraordinary wave reflection trace was not distinctly visible [*Nelms and Lockwood*, 1967; *Hagg*, 1967]. The inclusion of these very low densities on Figure 12 would lower the Alouette/ISIS density curve by an order of magnitude above 1.2 R_E. This would reduce the discrepancy between the low-altitude density studies and the observed DE 1 density values, since the whistler mode frequency cutoff method of determining electron densities is valid for low densities (see Figure 10). A more complete analysis of available topside ionograms would be necessary in order to determine an accurate slope of the electron density profile between 1.24 R_E and 1.47 R_E.

7. DISCUSSION AND SUMMARY

Electron densities at 2.0–4.66 R_E have been derived from the plasma frequency cutoff of the whistler mode radiation in the polar cap by using electric field spectrum measurements from the plasma wave instrument on the DE 1 spacecraft. A log-log plot of the median density values as a function of radial distance indicates a power law distribution of electron densities, varying as $R^{-3.85 \pm 0.32}$. This power law distribution is consistent with a steady state, radial outflow of ionospheric ions and electrons along polar magnetic field lines. It implies a nearly linear increase in plasma flow velocity with increasing radial distance at radial distances above 2 R_E.

A comparison of observed electron densities with theoretical ion and electron densities based on the classic polar wind model for supersonic ion flow velocities yields consistent results at 2.5–2.8 R_E. The theoretical polar wind densities below 2.5 R_E are slightly lower than the observed median densities. This result is not unexpected, since conditions of steady state plasma flow are not expected to exist across the polar cap at all latitudes and at all times.

A comparison of observed electron densities with low-altitude density profiles from the Alouette/ISIS topside sounder data indicates several evolutions in the radial dependence of electron distributions in the polar cap. A state of near diffusive equilibrium combined with an outward flux of plasma at subsonic transport speeds below 1000 km changes to a collision-dominated outward flux of plasma with a transition to supersonic velocities above 1000 km. This transition is clearly evident in the low-altitude density profile at approximately 1.16 R_E (see Figure 12). A second transition is also indicated in the density data gap between 1.55 R_E and 2.0 R_E to account for the changing nature of the density profiles at high and low altitudes in the polar cap. This second transition in the density profile is believed to be due to a change from a collision-dominated radial outflow distribution model below 1.5 R_E to a collisionless power law distribution above 2.0 R_E. Other factors affecting the change in the radial dependence of the electron number density include changes in the ionic composition of the plasma as well as changes in the plasma flow velocity and plasma temperature.

Large variations seen in low-altitude electron densities in earlier studies persist at the higher altitudes of the DE 1 orbit. The spread in the density data is the result of averaging over all polar magnetic latitudes and nearly 80 polar passes for the 5-month time interval of this study. Such a survey would conceal all density irregularities on a short time scale and would even suppress irregularities of large spatial dimensions which

are not consistent across the polar cap at a constant radial distance. Such irregularities in the density profile at low altitudes were discovered by the early topside sounder satellites. Alouette I, in a polar orbit at a constant radial distance of 1.16 R_E, provided evidence of latitudinal, diurnal, and seasonal variations in the electron density profile at high geomagnetic latitudes [*Nelms*, 1966; *Thomas et al.*, 1966]. Superimposed on the monotonic decrease in number density with increasing latitude were prominent peaks and troughs in the density distribution on spatial scales of several hundred kilometers [*Thomas et al.*, 1966]. In addition, many small-scale irregularities in space and time contributed to the spread in the density data. Some large-scale irregularities persisted over continuous polar passes in narrow bands of invariant latitude [*Sato and Colin*, 1969; *Chan and Colin*, 1969]. In general, polar cap density distributions were found to be very irregular and to sensitively depend on magnetic activity, seasonal variations, and local time.

Similar irregularities in the density profile are expected to persist at DE 1 altitudes. The previously cited examples of density profile variability between successive polar passes (see Figures 4–8) are evidence of large density fluctuations in time periods of less than 8 hours. Such a large transformation in the density profile for the same region of the polar magnetosphere is probably due to abrupt changes in the magnetic field activity. Sufficient data to examine seasonal variations in the density profile at DE 1 altitudes are not yet available. Statistically significant density data for seasonal comparisons at the same radial distances in the polar magnetosphere cannot be obtained until the DE 1 orbit has precessed around to the northern polar cap region in the spring of 1985. But sufficient density data already exist to investigate latitudinal density variations in the polar cap region and to compare these results with low-altitude studies of latitudinal density variations in order to determine the radial extent of persistent maxima and minima in the electron density distributions. A further comparison of magnetic activity and the density profile as a function of time is planned in order to determine the magnitude of the effect of magnetic convection on the electron density distribution at high geomagnetic latitudes and high altitudes.

REFERENCES

Axford, W. I., The polar wind and the terrestrial helium budget, *J. Geophys. Res., 73*, 6855, 1968.

Banks, P. M., and T. E. Holzer, The polar wind, *J. Geophys. Res., 73*, 6846, 1968.

Banks, P. M., and T. E. Holzer, Features of plasma transport in the upper atmosphere, *J. Geophys. Res., 74*, 6304, 1969a.

Banks, P. M., and T. E. Holzer, High-latitude plasma transport: The polar wind, *J. Geophys. Res., 74*, 6317, 1969b.

Bauer, S. J., Diffusive equilibrium in the topside ionosphere, *Proc. IEEE, 57*, 1114, 1969.

Brace, L. H., H. G. Mayr, and K. K. Mahajan, A polar maximum of electron concentration at 1000 km altitude, *J. Atmos. Terr. Phys., 32*, 1945, 1970.

Calvert, W, The auroral plasma cavity, *Geophys. Res. Lett., 8*, 919, 1981.

Calvert, W., and T. E. Van Zandt, Fixed-frequency observations of plasma resonances in the topside ionosphere, *J. Geophys. Res., 71*, 1799, 1966.

Chan, K. L., and L. Colin, Global electron density distributions from topside soundings, *Proc. IEEE, 57*, 990, 1969.

Chappell, C. R., J. L. Green, J. F. E. Johnson, and J. H. Waite, Jr., Pitch angle variations in magnetospheric thermal plasma—Initial observations from Dynamics Explorer 1, *Geophys. Res. Lett., 9*, 933, 1982a.

Chappell, C. R., R. C. Olsen, J. L. Green, J. F. E. Johnson, and J. H. Waite, Jr., The discovery of nitrogen ions in the earth's magnetosphere, *Geophy. Res. Lett., 9*, 937, 1982b.

Chen, F. F., *Introduction to Plasma Physics*, p. 116, Plenum, New York, 1974.

Dessler, A. J., and F. C. Michel, Plasma in the geomagnetic tail, *J. Geophys. Res., 71*, 1421, 1966.

Donley, J. L., L. H. Brace, J. A. Findlay, J. H. Hoffman, and G. L. Wrenn, Comparison of results of Explorer XXXI direct measurement probes, *Proc. IEEE, 57*, 1078, 1969.

Dungey, J. W., Interplanetary magnetic field and the auroral zones, *Phys. Rev. Lett., 6*, 47, 1961.

Florida, C. D., The development of a series of ionospheric satellites, *Proc. IEEE, 57*, 867, 1969.

Frank, L. A., J. D. Craven, J. L. Burch, and J. D. Winningham, Polar views of the earth's aurora with Dynamics Explorer, *Geophys. Res. Lett., 9*, 1001, 1982.

Gallagher, D. L., and D. A. Gurnett, Auroral kilometric radiation: Time-averaged source position, *J. Geophys. Res., 84*, 6501, 1979.

Gurgiolo, C., and J. L. Burch, DE 1 observations of the polar wind— A heated and an unheated component, *Geophys. Res. Lett., 9*, 945, 1982.

Gurnett, D. A., The earth as a radio source: Terrestrial kilometric radiation, *J. Geophys. Res., 79*, 4227, 1974.

Gurnett, D. A., and L. A. Frank, Plasma waves in the polar cusp: Observations from Hawkeye 1, *J. Geophys. Res., 83*, 1447, 1978.

Gurnett, D. A., S. D. Shawhan, and R. R. Shaw, Auroral hiss, Z mode radiation, and auroral kilometric radiation in the polar magnetosphere: DE 1 observations, *J. Geophys. Res., 88*, 329, 1983.

Hagg, E. L., Electron densities of 8–100 electrons cm^{-3} deduced from Alouette II high-latitude ionograms, *Can. J. Phys., 45*, 27, 1967.

Hoffman, J. H., Ion mass spectrometer on Explorer XXXI satellite, *Proc. IEEE, 57*(6), 1063, 1969.

Hoffman, J. H., and W. H. Dodson, Light ion concentrations and fluxes in the polar regions during magnetically quiet times, *J. Geophys. Res., 85*, 626, 1980.

Jackson, J. E., and E. S. Warren, Objectives, history, and principal achievements of the topside sounder and Isis programs, *Proc. IEEE, 57*, 861, 1969.

Knight, P., A classification of night-time electron-density profiles, *J. Atmos. Terr. Phys., 34*, 401, 1972.

Lin, C. S., J. L. Burch, S. D. Shawhan, and D. A. Gurnett, Correlation of auroral hiss and upward electron beams near the polar cap, *J. Geophys. Res., 88*, in press, 1983.

Maeda, K., Mid-latitude electron density profile as revealed by rocket experiments, *J. Geomagn. Geoelectr., 21*, 557, 1969.

Maeda, K., Study on electron density profile in the lower ionosphere, *J. Geomagn. Geoelectr., 23*, 133, 1971.

Miller, N. J., and L. H. Brace, Some winter characteristics of the northern high-latitude ionosphere, *J. Geophys. Res., 74*, 5752, 1969.

Mozer, F. S., C. A. Cattell, M. Temerin, R. B. Torbert, S. Von Glinski, M. Woldorff, and J. Wygant, The dc and ac electric field, plasma density, plasma temperature, and field-aligned current experiments on the S3-3 satellite, *J. Geophys. Res., 84*, 5875, 1979.

Nelms, G. L., Seasonal and diurnal variations of the distribution of electron density in the topside of the ionosphere, in *Electron Density Profiles in the Ionosphere and Exosphere*, edited by J. Frihagen, p. 358, North-Holland, Amsterdam, 1966.

Nelms, G. L., and G. E. K. Lockwood, Early results from the topside sounder in the Alouette II satellite, *Space Res.*, *7*, 604, 1967.

Raitt, W. J., Polar ionospheric measurements from the ESRO 1 satellite, *Space Res.*, *11*, 1147, 1971.

Raitt, W. J., R. W. Schunk, and P. M. Banks, A comparison of the temperature and density structure in high and low speed thermal proton flows, *Planet. Space Sci.*, *23*, 1103, 1975.

Reddy, B. M., D. R. Takshmi, and L. H. Brace, Response of the 1000-km ionosphere to magnetic storms, *Radio Sci.*, *4*, 851, 1969.

Sato, T., and L. Colin, Morphology of electron concentration enhancement at a height of 1000 km at polar latitudes, *J. Geophys. Res.*, *74*, 2193, 1969.

Sayers, J., J. W. G. Wilson, and B. Loftus, Anomalous features of the electron density in the topside ionosphere, *Proc. R. Soc. London Ser. A*, *311*, 501, 1969.

Schunk, R. W., and D. S. Watkins, Electron temperature anisotropy in the polar wind, *J. Geophys. Res.*, *86*, 91, 1981.

Schunk, R. W., and D. W. Watkins, Proton temperature anisotropy in the polar wind, *J. Geophys. Res.*, *87*, 171, 1982.

Shawhan, S. D., and D. A. Gurnett, The polarization of auroral kilometric radiation by Dynamics Explorer 1, *Geophys. Res. Lett.*, *9*, 913, 1982.

Shawhan, S. D., D. A. Gurnett, D. L. Odem, R. A. Helliwell, and C. G. Park, The plasma wave and quasi-static electric field instrument (PWI) for Dynamics Explorer-A, *Space Sci. Instrum.*, *5*, 535, 1981.

Shelley, E. G., W. K. Peterson, A. G. Ghielmetti, and J. Geiss, The polar ionosphere as a source of energetic magnetospheric plasma, *Geophys. Res. Lett.*, *9*, 941, 1982.

Stix, T. H., *The Theory of Plasma Waves*, pp. 30–32, McGraw-Hill, New York, 1962.

Thomas, J. O., M. J. Rycroft, L. Colin, and K. L. Chan, Experimental results from the Alouette I satellite, in *Electron Density Profiles in the Ionosphere and Exosphere*, edited by J. Frihagen, p. 322, North-Holland, Amsterdam, 1966.

Thrane, E. V., Information on the *D* and *E* region electron density profiles, *Radio Sci.*, *7*, 143, 1972.

Timleck, P. L., and G. L. Nelms, Electron densities less than 100 electrons cm^{-3} in the topside ionosphere, *Proc. IEEE*, *57*, 1164, 1969.

Tulunay, Y., Some topside electron density measurements from Ariel III satellite during the geomagnetic storm of 25–27 May 1967, *Planet. Space Sci.*, *20*, 1299, 1972.

D. A. Gurnett, A. M. Persoon, and S. D. Shawhan, Department of Physics and Astronomy, The University of Iowa, Iowa City, IA 52242.